# Prediction of the Electronic Structure via Molecular Stacking Mode of Radical Cation Salts Based on Asymmetric Donor Molecule MeEDO-TTF

Xiangfeng Shao,*[,†,‡] Yukihiro Yoshida,[§] Yoshiaki Nakano,[†,||] Hideki Yamochi,*[,†,‡] Masafumi Sakata,[§] Mitsuhiko Maesato,[§] Akihiro Otsuka,[†] Gunzi Saito,[§,⊥] and Shin-ya Koshihara[‡,#]

*Research Center for Low Temperature and Materials Sciences, Kyoto University, Sakyo-ku, Kyoto 606-8501, Japan, Non-equilibrium Dynamics Project, ERATO, Japan Science and Technology Agency, c/o KEK, 1-1 Oho, Tsukuba, Ibaraki, 305-0801, Japan, Division of Chemistry, Graduate School of Science, Kyoto University, Sakyo-ku, Kyoto 606-8502, Japan, Institute for Integrated Cell-Material Sciences (iCeMS), Kyoto University, Sakyo-ku, Kyoto 606-8501, Japan, Research Institute, Meijo University, Tempaku-ku, Nagoya 468-8502, Japan, and Frontier Collaborative Research Center & Department of Materials Science, Tokyo Institute of Technology, 2-12-1 Oh-okayama, Meguro-ku, Tokyo 152-8551, Japan*

*Received November 24, 2008. Revised Manuscript Received January 19, 2009*

By the electrochemical oxidation of 4,5-ethylenedioxy-4′-methyl-tetrathiafulvalene (MeEDO-TTF), six kinds of radical cation salts were prepared: three polymorphs of 2:1 $ReO_4^-$ salts, 4:1 $HCTMM^{2-}$ salt, and 5:2 salts with $CoCl_4^{2-}$ and $MnCl_4^{2-}$, where $HCTMM^{2-}$ denotes hexacyanotrimethylenemethanediide dianion. Among them, two modifications of $ReO_4^-$ salts showed metal−insulator transitions, while the other salts exhibited semiconducting or insulating behaviors in the measured temperature region. The crystal structures of these salts were successfully solved except for the powder polymorph of $ReO_4^-$ salt. In these crystals, the donor molecules formed *head-to-tail* stacking with the "ring-over-ring" and/or "ring-over-bond" type overlap modes along with the intermediate one between these two modes. The magnitudes of the face-to-face intermolecular interactions were greatly enhanced compared with those observed in the previously reported $(MeEDO\text{-}TTF)_2X$ ($X = BF_4^-$, $ClO_4^-$, $PF_6^-$), for which the *head-to-head* type molecular stacking with "ring-over-bond" overlap mode afforded two-dimensional Fermi surfaces. By contrast, the head-to-tail type stacking of MeEDO-TTF provided the quasi-one-dimensional electronic structure in the columnar stacks or localized charge carriers in the multimers. In the radical cation salts of the asymmetric donor molecule, MeEDO-TTF, the dimensionality of the electronic structure is greatly dependent on the molecular stacking types, head-to-head or head-to-tail.

## Introduction

In the molecular conductors, tetrathiafulvalene (TTF) and its derivatives are the most studied components, which have provided a number of radical cation salts with different types of electronic ground states.[1,2] It has been widely accepted that the electronic structures of the molecular conductors based on TTF derivatives can be predicted from the intermolecular interactions of their highest occupied molecular orbitals (HOMOs).[3,4] Systematic studies of the relationship between the relative orientation of neighboring donor molecules and electronic structures have been carried out especially for bis(ethylenedithio)−TTF (ET) radical cation salts.[5] (Scheme 1). The geometric relationship between the neighboring ET molecules governs the intermolecular interaction, which determines the electronic structure of the salt. This means that the intermolecular overlap mode plays the decisive role in determining the electronic properties of the salt.[5] In the radical cation salts of ET, the intermolecular overlap modes of "ring-over-bond" (RoB) and "ring-over-atom" (RoA) have been widely observed in the ET columns or layers (the schematic representation of each mode will appear subsequently, e.g., Figures 1 and 4).

Among the TTF derivatives, ethylenedioxy substituted compounds are of interest. Bis(ethylenedioxy)–TTF (BO) has afforded a variety of radical cation salts, most of which

* Corresponding author. E-mail: yamochi@kuchem.kyoto-u.ac.jp (H.Y.); shao_xf@kuchem.kyoto-u.ac.jp (X.S.).
† Research Center for Low Temperature and Materials Sciences, Kyoto University.
‡ Japan Science and Technology Agency.
§ Graduate School of Science, Kyoto University.
|| Institute for Integrated Cell-Material Sciences (iCeMS), Kyoto University.
⊥ Meijo University.
# Tokyo Institute of Technology.

(1) (a) Jérome, D.; Schulz, H. J. *Adv. Phys.* **1982**, *31*, 299–490. (b) Williams, J. M.; Ferraro, J.; Thorn, R. J.; Carlson, K. D.; Geiser, U.; Wang, H.-H.; Kini, A. M.; Wangbo, M. H.; *Organic Superconductors (including Fullerenes)*; Prentice Hall: Englewood Cliffs, NJ, 1992. (c) Ishiguro, T.; Yamaji, K.; Saito, G. *Organic Superconductors*, 2nd ed.; Spring-Verlag: Berlin, 1998.
(2) For comprehensive review, see: (a) *Chem. Rev.* **2004**, *104* (11). (b) *J. Phys. Soc. Jpn.* **2006**, *75* (5).
(3) (a) Minot, C.; Louie, S. G. *Phys. Rev. B* **1982**, *26*, 4793–4796. (b) Grant, P. M. *Phys. Rev. B* **1982**, *26*, 6888–6895. (c) Mori, T.; Kobayashi, A.; Sasaki, Y.; Kobayashi, H.; G. Saito, G.; Inokuchi, H. *Bull. Chem. Soc. Jpn.* **1984**, *57*, 627–633.
(4) Saito, G.; Yoshida, Y. *Bull. Chem. Soc. Jpn.* **2007**, *80*, 1–137.
(5) (a) Mori, T. *Bull. Chem. Soc. Jpn.* **1998**, *71*, 2509–2526. (b) Mori, T. *Bull. Chem. Soc. Jpn.* **1999**, *72*, 179–197. (c) Mori, T. *Bull. Chem. Soc. Jpn.* **1999**, *72*, 2011–2027.

10.1021/cm803180x CCC: $40.75 
Published on Web 02/27/2009

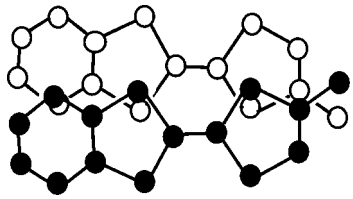

**Figure 1.** RoA type intermolecular overlap mode of the donor molecules in $(MeDO\text{-}TTF)_2X$ ($X = BF_4^-$, $ClO_4^-$, $PF_6^-$). The stereoview of the overlap mode is shown in Figure S1 in Supporting Information.

**Scheme 1**

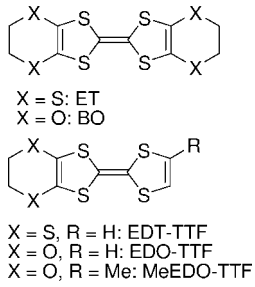


exhibited stable metallic behaviors down to cryogenic temperature.[6] As a result of the self-assembling nature of the BO molecule, the neighboring donor molecules in the pseudo-stacking direction slip along the molecular short axis to show RoA type overlap mode. The resultant so-called $\beta''$-type donor packing[5] benefits the formation of two-dimensional (2D) electronic structures. When one of the ethylenedioxy groups was removed to afford an asymmetric donor molecule, 4,5-ethylenedioxy−TTF (EDO-TTF), however, the radical cation salts showed various packing motifs and the BO-type self-assembling nature was significantly diminished. To classify the donor packing patterns of the asymmetric molecules, the relative orientation of the molecules must be concerned: *head-to-tail* and *head-to-head* types. In $(EDO\text{-}TTF)_2PF_6$, the gigantic photoresponse of which has attracted much attention,[7] the donor molecules formed head-to-tail face-to-face stacking with RoB type overlap mode to provide quasi-one-dimensional (Q1D) metal at room temperature.[8] In the crystal of $(EDO\text{-}TTF)_2X$ ($X = GaCl_4^-$, $ReO_4^-$), on the other hand, the donor molecules formed two kinds of layers with different band structures.[9] In one layer, the donor molecules exhibited head-to-tail face-to-face stacking to afford Q1D Fermi surface. In another layer, the donor molecules were twisted with respect to neighboring ones within the head-to-head stacking, resulting in the formation of a 2D Fermi surface.

In the other asymmetric TTF analogues with a relatively small $\pi$-electron system, such as 4,5-ethylenedithio−TTF (EDT-TTF),[10] 4,5-dimethyl−TTF (DMTTF),[11] 4,5-ethylenedioxy-4′,5′-dimethyl-tetraselenafulvalene (DMEDO-TSeF),[12] or asymmetric 2,5-bis(1,3-dithiol-2-ylidene)-1,3,4,6-tetrathiapentalene (BDT-TTP) derivatives,[13] the donor molecules formed the conducting layer mainly showing head-to-tail or the mixture of head-to-tail and head-to-head stackings with the RoB overlap mode. However, until recently, no conducting layer built up only with head-to-head type stacking has been reported in the radical cation salts of these donors to the best of our knowledge. Therefore, it is difficult to clarify the difference between the electronic structures of the donor layers consisted only of head-to-head and only of head-to-tail stackings for these asymmetric donor molecules.

When one methyl group was introduced to EDO-TTF to provide 4′-methyl-EDO-TTF (MeEDO-TTF), the radical cation salts showed various transport properties. Among them, the conducting layers in the highly conducting salts, $(MeEDO\text{-}TTF)_2X$ ($X = BF_4^-$, $ClO_4^-$, and $PF_6^-$), exhibited the same packing pattern which purely consisted of the head-to-head type pseudocolumns. The RoA overlap mode was observed along the stacking direction as depicted in Figure 1 (to show overlap modes, two neighboring donor molecules were projected onto the molecular best plane throughout this

(6) (a) Horiuchi, S.; Yamochi, H.; Saito, G.; Sakaguchi, K.; Kusunoki, M. *J. Am. Chem. Soc.* **1996**, *118*, 8604–8622. (b) Yamochi, H. In *TTF Chemistry Fundamental and Application of Tetrathiafulvalene*; Yamada, J., Sugimoto, T., Eds.; Kodansha Springer: Tokyo, **2004**, Chapter 4.

(7) (a) Uchida, N.; Koshihara, S.; Ishikawa, T.; Ota, A.; Fukuya, H. S.; Collet, M.; Yamochi, H.; Saito, G. *J. Phys. IV France* **2004**, *114*, 143–145. (b) Collet, M.; Guerin, L.; Uchida, N.; Fukuya, S.; Shimoda, H.; Ishikawa, T.; Matsuda, K.; Hasegawa, T.; Ota, A.; Yamochi, H.; Saito, G.; Tazaki, R.; Adachi, S.; Koshihara, S. *Science* **2005**, *307*, 86–89. (c) Koshihara, S.; Adachi, S. *J. Phys. Soc. Jpn.* **2005**, *75*, 011005/1−10.

(8) (a) Ota, A.; Yamochi, H.; Saito, G. *J. Mater. Chem.* **2002**, *12*, 2600–2602. (b) Ota, A.; Yamochi, H.; Saito, G. In *Multifunctional Conducting Molecular Materials*; Saito, G., Wudl, F., Haddon, R. C., Tanigaki, K., Enoki, T., Katz, H. E., Maesato, M., Eds.; RSC Publishing: Cambridge, U.K., 2007; pp 115−118.

(9) Ota, A.; Yamochi, H.; Saito, G. *J. Low Temp. Phys.* **2006**, *142*, 425–428.

(10) (a) Terzis, A.; Hountas, A.; Papavassilliou, G. C. *Solid State Commun.* **1988**, *66*, 1161–1162. (b) Terzis, A.; Hountas, A.; Underhill, A. E.; Clark, A.; Kaye, B.; Hilti, B.; Mayer, C.; Pfeiffer, J.; Yiannopoulos, S. Y.; Mousdis, G.; Papavassiliou, G. C. *Synth. Met.* **1998**, *27*, B97–B102. (c) Papavassiliou, G. C.; Mousdis, G. A.; Zambounis, J. S.; Terzis, A.; Houndas, A.; Hilti, B.; Meyer, C. W.; Pfeiffer, J. *Synth. Met.* **1998**, *27*, B379−B383. (d) Kato, R.; Kobayashi, H.; Kobayashi, A. *Chem. Lett.* **1989**, 781–784. (e) Kato, R.; Kobayashi, H.; Kobayashi, A.; Naito, T.; Tamura, M.; Tajima, H.; Kuroda, H. *Chem. Lett.* **1989**, 1839–1842. (f) Mori, T.; Inokuchi, H. *Solid State Commun.* **1989**, *70*, 823–827. (g) Hountas, A.; Terzis, A.; Papavassiliou, G. C.; Hilti, B.; Pfeiffer, J. *Acta Crystallogr.* **1990**, *C46*, 220–223. (h) Terzis, A.; Hountas, A.; Papavassiliou, G. C.; Hilti, B.; Pfeiffer, J. *Acta Crystallogr.* **1990**, *C46*, 224–228. (i) Hountas, A.; Terzis, A.; Papavassiliou, G. C.; Hilti, B.; Burkle, M.; Meyer, C. W.; Zambounis, J. *Acta Crystallogr.* **1990**, *C46*, 228–231. (j) Kikuchi, K.; Mochiduki, I.; Yamada, A.; Saitoh, H.; Saito, K.; Ikemoto, I.; Muraia, K. *Synth. Met.* **1991**, *41−43*, 1921–1924. (k) Biberacher, W.; Muller, H.; Heidmann, C.-P.; Probst, C. H.; Lerf, A.; Andres, K.; Kakoussis, V. C.; Papavassiliou, G. C.; Riede, J.; Hummel, H. U. *Synth. Met.* **1991**, *41−43*, 2377–2380. (l) Okano, Y.; Sawa, H.; Aonuma, S.; Kato, R. *Chem. Lett.* **1993**, 1851–1854. (m) Kato, R.; Yamamoto, K.; Tajima, H. *Chem. Commun.* **1997**, 947–948.

(11) (a) Uzelmeier, C. E.; Fourmigué, M.; Dunbar, K. R. *Acta Crystallogr.* **1998**, *C54*, 1047–1049. (b) Mhanni, A.; Ouahab, L.; Grandjean, D. *Acta Crystallogr.* **1993**, *C49*, 1187–1189. (c) Perepichka, I. F.; Perepichka, D. F.; Lyubchik, S. B.; Bryce, M. R.; Batsanov, A. S.; Howard, J. A. K. *J. Chem. Soc., Perkin Trans. 2* **2001**, 1546.

(12) (a) Shirahata, T.; Kibune, M.; Imakubo, T. *J. Mater. Chem.* **2005**, *15*, 4399–4402. (b) Shirahata, T.; Kibune, M.; Imakubo, T. *Chem. Commun.* **2006**, 1592–1594. (c) Shirahata, T.; Kibune, M.; Yoshino, H.; Imakubo, T. *Chem. Eur. J.* **2007**, *13*, 7619–7630.

(13) (a) Misaki, Y.; Kawakami, K.; Fujiwara, H.; Yamabe, T.; Mori, T.; Mori, H.; Tanaka, S. *Chem. Lett.* **1995**, 1125–1126. (b) Misaki, Y.; Kawakami, K.; Fujiwara, H.; Mimura, T.; Kochi, T.; Taniguchi, M.; Yamabe, T.; Mori, T.; Mori, H.; Tanaka, S. *Mol. Cryst. Liq. Cryst.* **1997**, *296*, 77–95. (c) Misaki, Y.; Fujiwara, H.; Maruyama, T.; Taniguchi, M.; Yamabe, T.; Mori, T.; Mori, H.; Tanaka, S. *Chem. Mater.* **1999**, *11*, 2360–2368.

**Table 1. Appearance, Composition, Optical Spectra, and Transport and Magnetic Properties of the Radical Cation Salts of MeEDO-TTF**

| | | | | | transport properties | | |
|---|---|---|---|---|---|---|---|
| entry | anion (A) | appearance | composition, D:A | optical bands[c], $10^3$ cm$^{-1}$ | $\sigma_{rt}$,[d] S cm$^{-1}$ | $E_a$,[e] meV | $\chi_{rt}$,[f] $10^{-4}$ emu mol$^{-1}$ |
| **1** | $ReO_4^-$ | powder | 2:1[a] | 3.4, 15.5, 21, 25 | 34 (MI)[g]<br>$T_{\sigma max}$[h] = 200 K | 20 at 180 K<br>50 at 150 K (max)<br>25 at 10 K | 2.5[j] |
| **2** | $ReO_4^-$ | plate | 2:1[b] | 3.4, 15.5, 20, 25 | 240 (MI)[i]<br>$T_{\sigma max}$[h] = 250 K | 14 at 220 K<br>300 at 150 K (max)<br>25 at 50 K | 3.8[k] |
| **3** | $ReO_4^-$ | needle | 2:1[b] | 3.4, 15.5, 21, 25 | $5 \times 10^{-3}$ (I)[i] | 200 at 300 K<br>160 at 200 K<br>50 at 115 K | –2.9[l] |
| **4** | $(HCTMM)^{2-}$ | thin plate | 4:1[a,b] | 3.4, 14, 25, 29 | 6 (S)[g] | 30 at 300 K<br>40 at 250 K (max)<br>35 at 200 K (min) | 1.3[j] |
| **5** | $(CoCl_4)^{2-}$ | plate | 5:2[b] | 5.5, 10, 13.5, 25 | $7 \times 10^{-4}$ (I)[i] | 250 (300−200 K) | 247[l] |
| **6** | $(MnCl_4)^{2-}$ | plate | 5:2[b] | 5.5, 10, 13.5, 25 | $3 \times 10^{-3}$ (I)[i] | 230 (300−200 K) | 287[l] |

[a] The composition (D: A) was estimated based on the elemental analysis. [b] The composition was determined by X-ray structure analysis. [c] Measured on the KBr pellet. [d] Room temperature conductivity (MI, metal-to-insulator transition system; I, Insulator; S, semiconductor). [e] Activation energy of electric conduction at the temperature indicated. [f] Room temperature magnetic susceptibility. [g] Measured on the compressed pellets. [h] The temperature where the conductivity reaches the maximum. [i] Measured on the single crystals. [j] After subtraction of core diamagnetism. [k] Determined based on the ESR signal intensity. [l] Without subtraction of core diamagnetism.

report).[14] In this case, the suppression of the face-to-face intermolecular interactions through the slip of the donor molecules along the molecular short axis gives rise to the formation of 2D electronic structures. In fact, the $BF_4^-$ and $ClO_4^-$ salts showed stable metallic behavior,[14a] while the $PF_6^-$ salt was a semiconductor due to the relatively weak intermolecular interactions.[14b]

In this work, we obtained a series of MeEDO-TTF radical cation salts only with head-to-tail type donor stacking. These salts enabled the effects of the relative orientation of the donor molecules on the physical properties of the salts to be evaluated. To verify the relationship between the molecular stacking manner and the electronic states of the salts, this article describes the structures and physical properties of the newly obtained head-to-tail type MeEDO-TTF salts and compares with those of the previously reported head-to-head type ones.

## Results and Discussion

**Composition and Optical Absorption Spectra.** Electrochemical oxidation of MeEDO-TTF in the presence of $(Bu_4N)ReO_4$ in EtOH afforded three kinds of radical cation salts in the form of black fine needles (denoted as powder **1**), bundles of black needle-like plates (denoted as plates **2**) and black needles (**3**) (see Figure S2 in Supporting Information). **1** and **2** were formed simultaneously at room temperature (rt) by applying a constant current of 0.5 $\mu$A. **3** can be obtained either at rt by applying higher current (>10 $\mu$A) or at low temperature (5 °C) by applying lower current (0.5 $\mu$A). These three modifications had the same compositions with the donor/anion ratio of 2:1. The composition of **1** was estimated on the basis of the elemental analysis, while those of **2** and **3** were confirmed by the X-ray structure analyses. Radical cation salt $(MeEDO\text{-}TTF)_4(HCTMM)$ ($HCTMM^{2-}$: hexacyanotrimethylenemethanediide dianion) (**4**) was prepared according to ref 14a. Electrocrystallization of MeEDO-TTF in the presence of $(Et_4N)_2CoCl_4$ and $(Et_4N)_2MnCl_4$ in EtOH provided the black plates of $(MeEDO\text{-}TTF)_5(CoCl_4)_2$ (**5**) and $(MeEDO\text{-}TTF)_5(MnCl_4)_2$ (**6**), respectively. The compositions of **5** and **6** were confirmed by the X-ray structure analyses.

The optical absorption spectra of all the radical cation salts in this study were measured by dispersing the salts in KBr pellets (Figure 2). The low-lying absorption band (A band) at around $3.4 \times 10^3$ cm$^{-1}$ was observed for **1**−**4**, while it did not definitely appear for **5** and **6** as in the case of the monocationic salt $(MeEDO\text{-}TTF)(FeBr_4)$. This band is ascribable to the intermolecular charge-transfer (CT) transition: $D^0 + D^{\bullet+} \rightarrow D^{\bullet+} + D^0$, where D indicates the donor molecule. The emergence of this band indicates the partially charged state of the donor molecules as an average. The optical spectra of the other highly conducting MeEDO-TTF radical cation salts also show this band.[14] The B band, which is defined as the intermolecular CT transition of $D^{\bullet+} + D^{\bullet+} \rightarrow D^{2+} + D^0$ and was observed at around $10 \times 10^3$ cm$^{-1}$ in $(MeEDO\text{-}TTF)(FeBr_4)$,[14b] was not observed in **1**−**4**. However, it appeared in **5** and **6** due to the dense charge on each donor molecule (+0.8 as average). The shoulder observed at $6 \times 10^3$ cm$^{-1}$ in **5** and **6** is most plausibly ascribable to the A band with weak intensity that appeared on the wing of the B band. The other higher energy absorption bands were assigned to the intramolecular transitions of the MeEDO-TTF radical cations. In the succeeding sections, the physical properties of each salt are described along with the crystal structure, when available.

**Physical Properties of Powder $(MeEDO\text{-}TTF)_2ReO_4$ (1).** The temperature-dependent resistivity ($\rho$) measurement of **1** was performed on the compressed pellet. **1** showed relatively good conductivity at room temperature ($\sigma_{rt}$) of 34 S cm$^{-1}$ and weak metallic behavior down to around 200 K, associated with a temperature-independent magnetic susceptibility $\chi$ (see Table 1, also Figure S3 in Supporting Information). At around 200 K, a metal-to-insulator (MI)

(14) (a) Shao, X.; Nakano, Y.; Yamochi, H.; Dubrovskiy, A. D.; Otsuka, A.; Murata, T.; Yoshida, Y.; Saito, G.; Koshihara, S. *J. Mater. Chem.* **2008**, *18*, 2131–2140. (b) Shao, X.; Nakano, Y.; Sakata, M.; Yamochi, H.; Yoshida, Y.; Maesato, M.; Uruichi, M.; Yakushi, K.; Murata, T.; Otsuka, A.; Saito, G.; Koshihara, S.; Tanaka, K. *Chem. Mater.* **2008**, *20*, 7551–7562.

**Table 2. Crystallographic Data, Data Collection, and Reduction Parameters of the Plate Modification of (MeEDO-TTF)$_2$ReO$_4$ (2) at Different Temperatures**

| | 300 K | 260 K | 220 K | 150 K |
|---|---|---|---|---|
| chemical formula | $C_{18}H_{16}O_8ReS_8$ | $C_{18}H_{16}O_8ReS_8$ | $C_{18}H_{16}O_8ReS_8$ | $C_{36}H_{32}O_{16}Re_2S_{16}$ |
| formula weight | 802.99 | 802.99 | 802.99 | 1605.98 |
| crystal system | triclinic | triclinic | triclinic | triclinic |
| space group | $P\bar{1}$ (No. 2) | $P\bar{1}$ (No. 2) | $P\bar{1}$ (No. 2) | $P\bar{1}$ (No. 2) |
| crystal size, mm$^3$ | 0.60 × 0.20 × 0.05 | 0.60 × 0.20 × 0.05 | 0.60 × 0.20 × 0.05 | 0.60 × 0.20 × 0.05 |
| $a$, Å | 7.332 (2) | 7.302 (1) | 7.272 (1) | 14.447 (1) |
| $b$, Å | 12.552 (3) | 12.531 (2) | 12.513 (1) | 12.496 (1) |
| $c$, Å | 14.943 (6) | 14.911 (2) | 14.880 (1) | 14.806 (1) |
| α, deg | 70.452 (9) | 70.475 (6) | 70.492 (5) | 70.521 (4) |
| $\beta$, deg | 82.256 (18) | 82.402 (7) | 82.574 (5) | 82.684 (4) |
| $\gamma$, deg | 89.115 (10) | 89.078 (7) | 89.032 (6) | 88.718 (5) |
| $V$, Å$^3$ | 1283.5 (7) | 1274.1 (3) | 1265.1 (2) | 2498.8 (3) |
| $Z$ | 2 | 2 | 2 | 2 |
| $\mu$, mm$^{-1}$ | 5.428 | 5.468 | 5.507 | 5.576 |
| $d_{calcd}$, g cm$^{-3}$ | 2.078 | 2.093 | 2.108 | 2.134 |
| radiation | Mo Kα | Mo Kα | Mo Kα | Mo Kα |
| $2\theta_{max}$, deg | 52 | 52 | 52 | 52 |
| no. of independent obsd reflections | 4556 | 4564 | 4520 | 9021 |
| no. of reflections with $I > 2\sigma(I)$ | 3294 | 3513 | 3712 | 6408 |
| no. of refined parameters | 391 | 391 | 391 | 768 |
| $wR2$[a] (for all data) | 0.199 | 0.155 | 0.162 | 0.178 |
| $R_{gt}$(%) (for $I > 2\sigma(I)$) | 0.059 | 0.053 | 0.054 | 0.070 |
| GOF[b] | 1.106 | 1.111 | 1.122 | 1.077 |

[a] $W = 1/[\sigma^2F_o^2 + (\alpha P)^2 + \beta P]$, where $P = (F_o^2 + 2F_c^2)/3$; at 150 K, α = 0.0445, $\beta$ = 32.8114; at 220 K, α = 0.0636, $\beta$ = 6.3740; at 260 K, α = 0.0536, $\beta$ = 5.7994; and at 300 K, α = 0.0836, $\beta$ = 5.6508. [b] Calculated for all of the independent reflections.

transition was observed. The magnetic and transport properties of this salt are similar to those of other MeEDO-TTF salts exhibiting MI transition, such as (MeEDO-TTF)$_2$X (X = $AsF_6^-$, $SbF_6^-$).[14a]

**Quasi-One-Dimensional Columns: Plate (MeEDO-TTF)$_2$ReO$_4$ (2).** The crystal structure of **2** was solved at different temperatures, and the crystallographic data are summarized in Table 2. Below 200 K, a structural transition was observed. Hereafter, the two distinct phases above and below 200 K are denoted as high- and low-temperature phases, respectively.

In the high-temperature phase, the asymmetric unit contained two donor molecules, **A** and **B**, and one anion. **2** consisted of layered structure: the conducting layers were built up of MeEDO-TTF radical cations and sandwiched along the $(-b + c)$ direction by layers of tetrahedral $ReO_4^-$ anion as shown in Figure 3a. The anion was severely disordered. The central Re atom occupied two positions with the site occupancy factor (s.o.f.) of 0.5 for each site at 300 K, but the s.o.f. of these two positions disproportionated on cooling, for example, 0.8 and 0.2 at 220 K. Even by assuming two orientations of the anion to express the rotational disorder, the equivalent temperature factor of each oxygen atom was rather large ($U_{eq}$ = 0.10−0.28).

In both crystallographically independent MeEDO-TTFs, the central TTF skeletons showed approximately planar shapes, whereas the methyl and ethylene groups exhibited the positional and flipping disorders, respectively. The s.o.f. for the two positions of the methyl groups were 0.7 and 0.3. The corresponding bonds in each donor molecule showed the same lengths within the estimated standard deviations.

The donor packing patterns and intermolecular overlap integrals for high- and low-temperature phases are shown in Figures 3b,c, respectively. The donor molecules stacked in the head-to-tail manner to form the one-dimensional

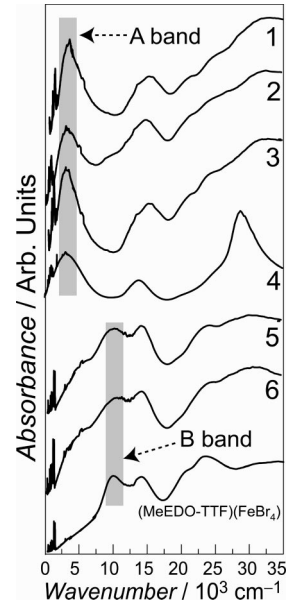


**Figure 2.** Optical absorption spectra of the radical cation salts in this study. The lines **1**−**6** show the spectra of powder (**1**), plate (**2**), and needle (**3**) forms of (MeEDO-TTF)$_2$ReO$_4$, (MeEDO-TTF)$_4$(HCTMM) (**4**), (MeEDO-TTF)$_5$(CoCl$_4$)$_2$ (**5**), and (MeEDO-TTF)$_5$(MnCl$_4$)$_2$ (**6**), respectively. The spectra are compared with that of the monocationic (MeEDO-TTF)(FeBr$_4$) salt.

columns along the $a$-axis. In the high-temperature phase, the intermolecular overlap modes of the two neighboring donor molecules in a unit cell (**A** and **B**) and in the adjacent unit cell (**A** and **B′**, where **B′** is derived from **B** by translation of $(1 + x, y, z)$) are shown in Figures 4a,b, respectively. The latter is so-called RoB type overlap mode,[5] where two donor molecules were shifted around one central C═C bond length along the molecular long axis. In the former case, however, two donor molecules only slightly shifted along the molecular long axis and approximately formed eclipsed configuration denoted as "ring-over-ring" (RoR) type overlap mode in this

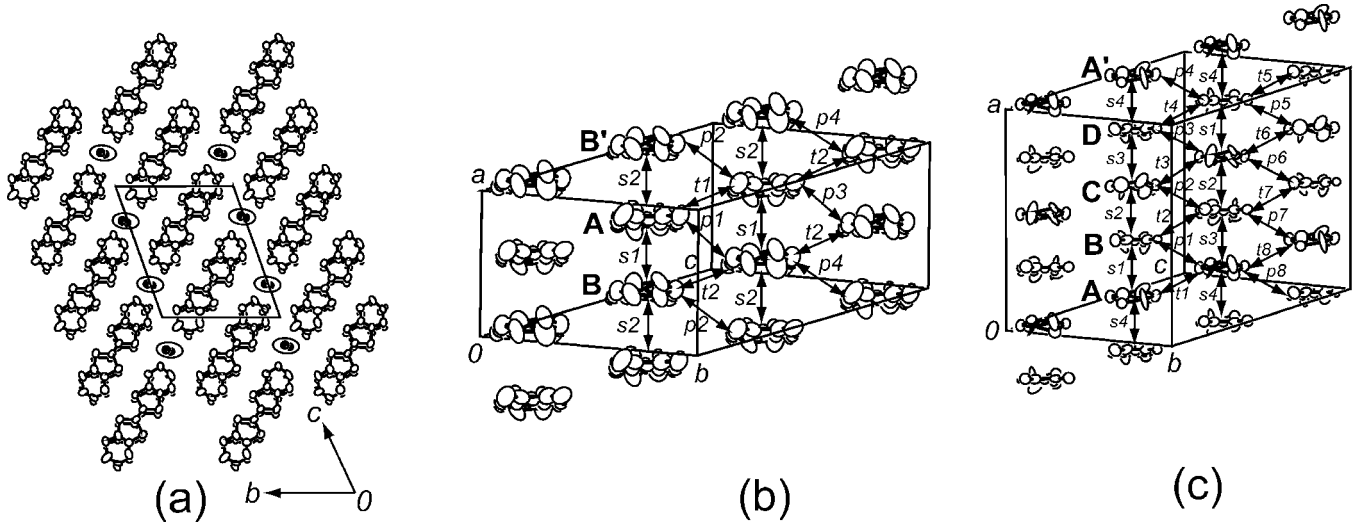


**Figure 3.** Crystal structure of **2**. The hydrogen atoms were omitted for clarity. (a) Projection along the *a*-axis at 300 K, where the ellipse indicates the positions of the anion. The long and short axes of a donor molecule correspond to the crystallograhpic $-b + c$ and $2b + c$ directions, respectively; (b) and (c) view of the donor layer along the molecular long axis with scheme of the intermolecular overlap integrals at 300 and 150 K, respectively. In (b), the crystallographically independent two donor molecules were marked with **A** and **B**, while **B′** was derived from **B** through the translation of $(1 + x, y, z)$. In (c), the crystallographically independent four donor molecules were marked with **A**, **B**, **C**, and **D**, while **A′** was derived from **A** through the translation of $(1 + x, y, z)$. At 300 K: $s1 = -29.4$, $s2 = -24.7$, $t1 = 3.3$, $t2 = 4.3$, $p1 = 2.7$, $p2 = 1.3$, $p3 = 3.2$, $p4 = 0.6 \times 10^{-3}$; at 150 K: $s1 = -36.8$, $s2 = -27.6$, $s3 = -25.2$, $s4 = -28.4$, $t1 = t4 = 3.94$, $t2 = t3 = 4.96$, $t5 = t8 = 4.60$, $t6 = t7 = 3.21$, $p1 = p3 = 3.41$, $p2 = p4 = 0.47$, $p5 = p7 = 1.05$, $p6 = p8 = 2.76 \times 10^{-3}$.

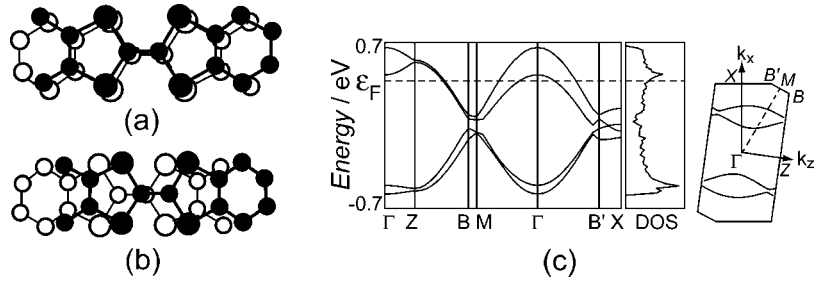


**Figure 4.** Intermolecular overlap modes of MeEDO-TTF in **2** at 300 K (see Figure S4 in Supporting Information for the stereoview); those at 150 K are shown in Figures S5 in Supporting Information. (a) RoR type overlap between **A** and **B**, corresponding to the overlap integral *s*1; (b) RoB type overlap between **A** and **B′**, corresponding to the overlap integral *s*2; (c) calculated band structure, density of states (DOS), and Fermi surface of **2** based on the crystal structure at 300 K.

article.[15] Although the RoR overlap mode has been observed in the TTF radical cation salts with halides or linear anion $NCS^-$,[16] it has been rarely observed in the CT complexes of the other TTF analogues.[11b,17] The intermolecular interaction in RoR is expected to be larger than that in RoB. In fact, the calculated intermolecular overlap integrals of RoR (*s*1) and RoB (*s*2) were 29.7 and 24.7 $\times 10^{-3}$, respectively. In this salt, the intracolumn intermolecular interactions (*s*1 and *s*2) were much larger than the intercolumn ones (*t*1, *t*2, *p*1, *p*2, *p*3, and *p*4). As a result, a Q1D electronic structure was formed.

In low-temperature phase, the unit cell was doubled along the stacking axis (*a*-axis) as shown in Figure 3c. The asymmetric unit contained four donor molecules and two anions, which were located on the general positions. The intermolecular overlap integrals along the stacking axis were split into four types: *s*1, *s*2, *s*3, and *s*4. Among them, *s*1 showed the largest value due to the RoR overlap mode, *s*2 and *s*4 showed nearly the same value in the overlap mode

(15) Note that in the literature this molecular stacking mode is also denoted as "atom-over-atom": (a) Brossard, L.; Ribault, M.; Garreau, B.; Pomarède, B.; Cassoux, P. *Europhys. Lett.* **1992**, *19*, 223–227. (b) Rosa, A.; Ricciardi, G.; Baerends, E. J. *Inorg. Chem.* **1998**, *17*, 1368–1379. (c) Fang, Q.; Xu, W.; Lei, H.; Xu, C. −Y.; Zhang, B.; Zhu, D. *Inorg. Chem. Commun.* **2004**, *7*, 1157–1160.

(16) For the examples of TTF radical cation salts or charge transfer complexes showing ring-over-ring intermolecular overlap mode: (a) Dahm, D. J.; Johnson, G. R.; May, F. L.; Miles, M. G.; Wilson, J. D. *Cryst. Struct. Commun.* **1975**, *4*, 673. (b) Sanz, F. *An. Fis.* **1976**, *72*, 43. (c) Johnson, C. K.; Watson, C. R., Jr. *J. Chem. Phys.* **1976**, *64*, 2271–2286. (d) Scott, B. A.; Placa, S. J. La.; Torrance, J. B.; Silverman, B. D.; Welber, B. *J. Am. Chem. Soc.* **1977**, *99*, 6631–6639. (e) Kobayashi, H.; Kobayashi, K. *Bull. Chem. Soc. Jpn.* **1977**, *50*, 3127. (f) Williams, R.; Ma, C. L.; Samson, S.; Khanna, S. K.; Somoano, R. B. *J. Chem. Phys.* **1980**, *72*, 3781–3788. (g) Teitelbaum, R. C.; Marks, T. J.; Johnson, C. K. *J. Am. Chem. Soc.* **1980**, *102*, 2986–2989. (h) Pyrka, G. J.; Fernando, Q.; Inoue, M. B.; Inoue, M. *Inorg. Chim. Acta* **1989**, *156*, 257. (i) Mizuno, M.; Kokudo, H.; Honda, K. *J. Mater. Chem.* **2001**, *11*, 2192. (j) Mercier, N.; Giffard, M.; Pilet, G.; Allain, M.; Hudhomme, P.; Mabon, G.; Levillain, E.; Gorges, A.; Riou, A. *Chem. Commun.* **2001**, 2722. (k) Giffard, M.; Marbon, G.; Leclair, E.; Mercier, N.; Allain, M.; Gorgues, A.; Molinié, P.; Neilands, O.; Krief, P.; Khodorkovsky, V. *J. Am. Chem. Soc.* **2001**, *123*, 3852–3853.

(17) (a) Although it was not discussed in ref 7a, in the low-temperature phase of $(EDO\text{-}TTF)_2PF_6$, the intermolecular overlap mode between two flat donor molecules is ring-over-ring type. For ET salt: (b) Perruchas, S.; Boubekeur, K.; Auban-Senzier, P. *J. Mater. Chem.* **2004**, *14*, 3509–3515. For bis(methylenedithio)tetrathiafulvalene salt: (c) Nigrey, P. J.; Morosin, B.; Kwak, J. F.; Venturini, E. L.; Baughman, R. J. *Synth. Met.* **1986**, *16*, 1–25.

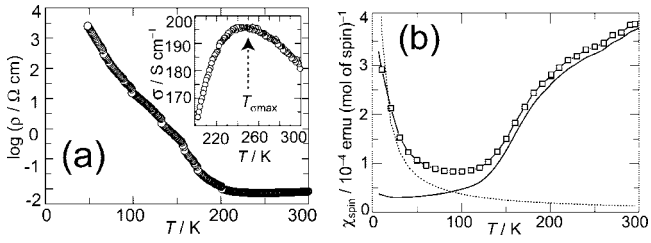


**Figure 5.** (a) Plot of resistivity ($\rho$) vs temperature ($T$) of **2**. The insert indicates the $T_{\sigma max}$; (b) plot of the spin susceptibility ($\chi_{spin}$) vs temperature ($T$) of **2** (□). The dashed and solid lines indicate the Curie term and the $\chi_{spin}$ after subtraction of Curie term, respectively.

of RoB, and $s3$ was the smallest one, where the two donor molecules were shifted around half of the central C═C bond length along the molecular longitudinal axis (see Figure S5 in Supporting Information). Therefore, the donor molecules were slightly tetramerized along the stacking direction through the interactions $s4-s1-s2$, where the intertetramer interaction was $s3$. Similar to the high-temperature phase, the intercolumn interactions were much smaller than those of the intracolumn ones. Note that the central Re atom of the anion still occupied two positions with the s.o.f of 0.9 and 0.1 at 150 K.

The tight-binding approximated calculation based on the crystal structure of the donor layer at 300 K resulted in the Q1D electronic structure as shown in Figure 4c. Associated with the doubling, a gap was formed at the Fermi level at 150 K (see Figure S6 in Supporting Information). The expected nesting vector mainly consists of the $a^*$-component, which well corresponds to the direction of the cell doubling. Thus, the structural transition at 200 K is most plausibly due to the Peierls instability.

The resistivity of **2** was measured on the single crystal along the crystal long axis, which corresponded to the stacking axis of donor molecules. Consistent with the calculated band structure, this salt showed metallic behavior down to 250 K as shown in Figure 5a. Below this temperature ($T_{\sigma max}$), on the other hand, semiconducting behavior with temperature-dependent activation energy ($E_a$) was observed. As a result of the difficulty in isolating enough **2**, magnetic susceptibility was estimated by employing ESR on a single crystal (for the detailed information of the ESR measurement, see Figures S7−S11 in Supporting Information). The spin susceptibility ($\chi_{spin}$) gradually decreased from room temperature to 200 K, while no anomaly was observed at $T_{\sigma max}$. Rapid increment in $\rho$ and decrement in $\chi_{spin}$ were observed below 200 K, in good agreement with the structural transition mentioned above. An upturn of $\chi_{spin}$ below 50 K followed the Curie law with the Curie constant of $3.7 \times 10^{-3}$ emu K (mol of spin)$^{-1}$, which corresponds to the spin concentration of approximately 1% of the $S = 1/2$ isolated spin (= 0.375 emu K (mol of spin)$^{-1}$).

**Donor Tetramers: Needle (MeEDO-TTF)$_2$ReO$_4$ (3) and (MeEDO-TTF)$_4$(HCTMM) (4).** Although the space groups were different, the structures of the donor layers and the calculated electronic structures of **3** and **4** showed similar features. Therefore, only those of **3** are discussed here, while those of **4** are shown in Figures S14−S18 in Supporting Information. In both cases, the accuracy of the analyses is not sufficient to discuss the details of the structures. In this report, only the donor molecule arrangements are discussed. In the crystal of **3**, four donor molecules **A**, **B**, **C**, and **D** and two anions are crystallographically unique. In a unit cell, the donor molecules formed two layers which were interrelated by the center of inversion and were alternated by the anion layer along the $c$-axis (Figure 6a). All of the four donors were approximately planar. No positional disorder of the methyl group was observed in the structural analysis, while both of the $ReO_4$ anions showed rotational disorder.

In the donor layers, the donor molecules formed tetramers which consisted of four independent molecules with head-to-tail manner as shown in Figure 6b. The tetramers showed two different orientations with a dihedral angle of approximately 90° to form a so-called $\kappa$-4 × 4 type donor packing pattern. This type of the donor packing pattern has been rarely reported in the organic cation radical salts.[18]

In a tetramer, the central two donor molecules, **B** and **C**, showed slight shift along the molecular long axis to exhibit RoR type overlap pattern (Figure 7a). However, the pair of **A** and **B**, as well as the one of **C** and **D**, formed RoB configuration (Figure 7b). Consequently, the intermolecular sulfur···sulfur atomic contacts shorter than the sum of the van der Waals radii (3.6 Å) were only observed between the central two donor molecules, **B** and **C**, within a tetramer. The intermolecular overlap integral between **B** and **C** ($s1$) was around 1.5 times larger than that between **A** and **B** ($s2$) as well as that between **C** and **D** ($s3$). As a result of the strong face-to-face overlap in the head-to-tail type molecular stacking, the intratetramer overlap integrals ($s1-3$) were much larger than the intertetramer ones ($t1-5$, and $p1-3$). Concerning the composition of this salt, a couple of spins is expected to be strongly confined in a tetramer. This picture is consistent with the singlet−triplet type temperature dependence of magnetic susceptibility as discussed later. Eight HOMO bands were substantially split due to the strong intratetramer interactions, and a band gap of 150 meV was found at the Fermi level, suggesting that **3** should be a band insulator.

The electric conductivity of **3** was measured on the single crystal. This salt showed semiconducting behavior in the whole temperature region measured (Figure 8a), in good agreement with the calculated band structure. The magnetic susceptibility ($\chi$) in the high temperature region showed thermally activated behavior with small magnitude at room temperature as shown in Figure 8b. The temperature dependence was well fitted to the singlet−triplet model, reflecting the formation of a couple of spin in a tetramer:[19]

$$\chi_{calcd} = f\frac{2N_A g^2 \mu_B}{k_B T}\frac{1}{3+\exp\left(-\frac{2J}{k_B T}\right)} + (1-f)\frac{C}{T} + A$$

where $N_A$ is the Avogadro number; $g$ is the isotropic $g$-factor (assumed to be 2); $k_B$ is the Boltzmann constant; $\mu_B$ is the Bohr magneton; and $C$ is the Curie constant. The fitting

(18) (a) Kobayashi, A.; Kato, R.; Naito, T.; Kobayashi, H. *Synth. Met.* **1993**, *55−57*, 2078–2083. (b) Xu, W.; Shen, R.; Liu, C.-M.; Zhang, D.; Zhu, D. *Synth. Met.* **2003**, *133−134*, 349–351.

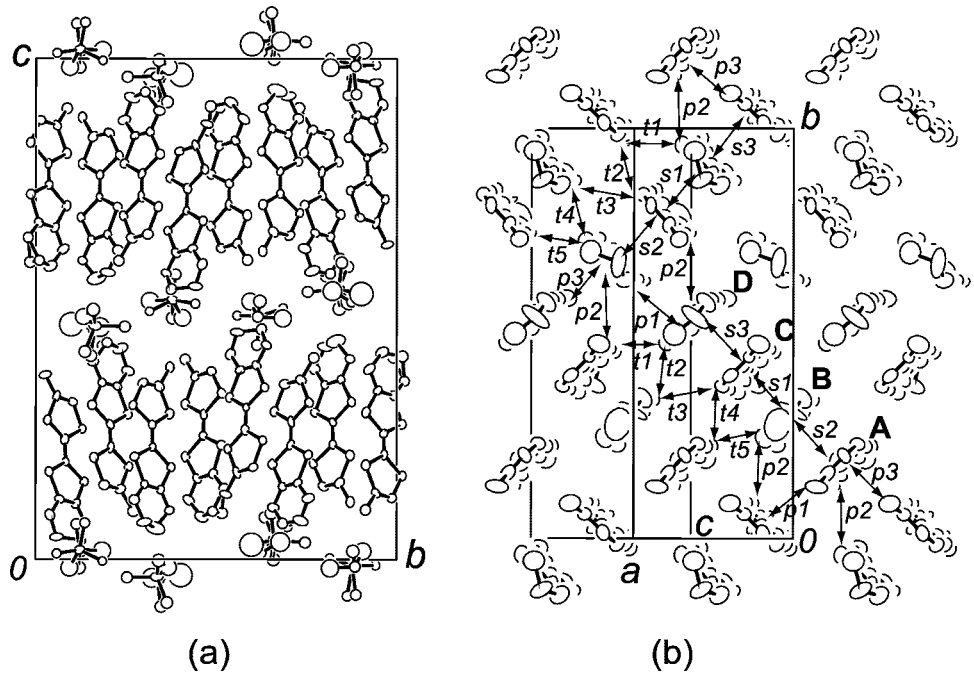


**Figure 6.** Crystal structures of **3**. The hydrogen atoms were omitted for clarity. (a) A unit cell projected along the *a*-axis (see Figure S12 in Supporting Information for the stereoview); (b) the donor layer at $z = 1/4$ projected along the molecular long axis with the scheme of the intermolecular interactions. **A**, **B**, **C**, and **D** indicate the crystallographically independent four donor molecules. $s1 = -38.0$, $s2 = 27.1$, $s3 = 24.0$, $p1 = -7.5$, $p2 = 7.6$, $p3 = -8.9$, $t1 = 11.4$, $t2 = 2.1$, $t3 = -5.1$, $t4 = 2.6$, $t5 = 12.3 \times 10^{-3}$.

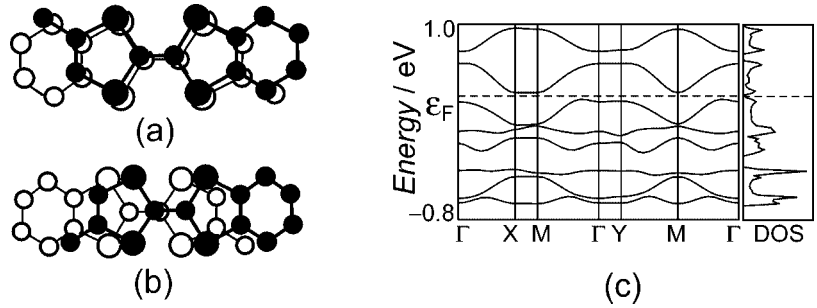


**Figure 7.** Intratetramer intermolecular overlap modes in **3** (see Figure S13 in Supporting Information for the stereoview). (a) RoR type overlap between two donor molecules **B** and **C**, corresponding to the intermolecular overlap *s*1; (b) RoB type overlap between two donor molecules **A** and **B** (and **C** and **D**), corresponding to the intermolecular overlap integral *s*2 (*s*3); (c) energy dispersion and DOS of **3**, the position of the Fermi energy ($\varepsilon_F$) is indicated by the dashed line.

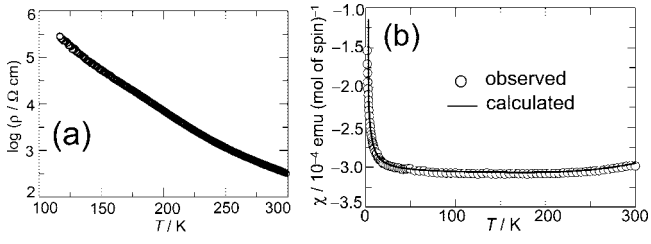


**Figure 8.** (a) Plot of the resistivity ($\rho$) vs temperature ($T$) of **3**; (b) plot of the magnetic susceptibility ($\chi$) vs temperature ($T$) of **3**, open circle and solid line indicate the observed and calculated $\chi$ values (see text), respectively.

parameters were determined as $A$, core diamagnetism term, $-3.11 \times 10^{-4}$ emu mol$^{-1}$, after subtraction of which the real $\chi$ at RT was $1.5 \times 10^{-5}$ emu (mol of spin)$^{-1}$; $f$, the molar fraction of the coupled spin, 0.999, indicating 0.1% of Curie spin; and $2J/k_B = -2000$ K, which corresponds to around 180 meV and is comparable to the activation energy (200 meV) estimated from the electric conduction measurement at around 300 K and the calculated band gap.

As mentioned above, the donor layers of **3** and **4** were approximately isostrcutural to each other. The latter salt also exhibited semiconducting behavior as reported in ref 14a (see also Figure S19 in Supporting Information), although it showed better conductivity with smaller activation energy for electric conduction than those of **3**.

**Coexistence of Donor Dimer and Monomer: (MeEDO-TTF)$_5$(MCl$_4$)$_2$ (M = Co (5) and Mn (6)).** In advance of the discussion of crystal structure, a brief statement of the vibrational spectra of **5** and **6** is given, while the detailed data for the vibrational spectra of MeEDO-TTF has been published separately.[14b] The IR spectra of these two salts are ascribable to the coexistence of the neutral and monocationic MeEDO-TTFs (Figure 9).

Since **5** and **6** were isostructural to each other, only the structural features and intermolecular interactions of **6** are

(19) (a) Kahn, O. *Molecular Magnetism*; Wiley-VCH: Weinheim, 1993. (b) Saito, G.; Pac, S. S.; Drozdova, O. O. *Synth. Met.* **2001**, *120*, 667–670. (c) Ito, A.; Nakano, Y.; Urabe, M.; Tanaka, K.; Shiro, M. *Eur. J. Inorg. Chem.* **2006**, 3359–3368.

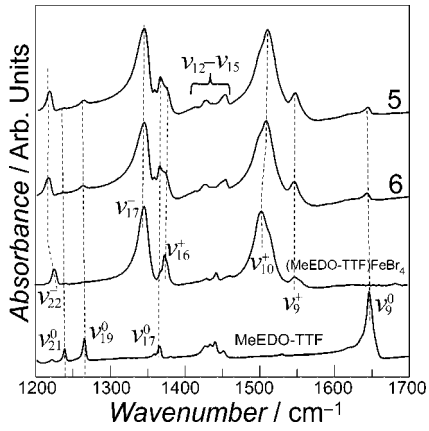


**Figure 9.** IR spectra of **5** and **6**. For reference, those of the neutral donor MeDO-TTF and monocationic salt (MeEDO-TTF)$FeBr_4$ are also shown. The spectra were measured on the KBr pellets. For the assignment of the vibritional bands, see ref 14b.

described (those of **5** are given in Supporting Information, Figures S22−S26). The asymmetric unit contained five donor molecules (**A**−**E**) and two anions. The crystal showed layered structure: the donor layers were sandwiched by the layers of the tetrahedral $MnCl_4^{2-}$ anions along the *c*-axis as shown in Figure 10a. All of the five donors were nearly planar. No positional disorder of the methyl group was observed in the structural analysis. Both of the crystallographically unique anions were ordered.

In the donor layer, the donor molecules formed two kinds of dimers, **A**-**B** and **C**-**D**, while the molecular mean plane of **E** was approximately perpendicular to those of molecules in the dimers (Figure 10b). In a dimer, two donor molecules showed head-to-tail stacking to form RoR type overlap as shown in Figure 11a. The intermolecular overlap integrals in a dimer ($s1$ and $s2$) were more than three times larger than the other ones.

Although the bond lengths of these five molecules showed similar values within the standard deviations, which were relatively large presumably due to the poor quality of the crystals, the vibrational spectra indicate the charge disproportionation in **6** as mentioned above. Since $MnCl_4^{2-}$ (also $CoCl_4^{2-}$) is a dianion, it is most plausible that each dimer possesses +2 charge, while the monomer is neutral. Assuming the energies of HOMOs are the same for all of the donor molecules in this salt, the calculated energy dispersion showed the gap at Fermi level (Figure 11b). The charge disproportionation should be reflected in the difference of HOMO energies in principle, which should mainly affect the energy level of the flattened band near to the Fermi level relative to those of other bands in the case of this salt. Since no band dispersion crosses the Fermi level, this salt should be a band insulator.

The electric conductivities of **5** and **6** were measured on the single crystals. Both of the salts exhibited semiconducting behavior with low conductivities and high activation energies (see Figure 12a and Table 1), consistent with the calculated band structure.

The magnetic susceptibilities of these two salts are shown in Figure 12b. As a result of the strong intradimer interactions ($s1 = 46 \times 10^{-3}$, $s2 = -45 \times 10^{-3}$), dimers should have a singlet ground-state even at room temperature, and they are expected to have approximately no contribution to the magnetism. The magnetic susceptibilities of **5** and **6** followed the Curie−Weiss law as shown in Figure 12b, with the Weiss temperatures of −3.8 and 1.5 K, respectively. The $\chi T$ values at room temperature for **5** and **6** were 7.44 and 8.40 emu K $mol^{-1}$, respectively. The latter is comparable fairly well with the theoretical $\chi T$ of 8.75 emu K $mol^{-1}$ for two isolated spins of $S = 5/2$ ($Mn^{2+}$) assuming $g = 2$. This confirms that the spin contribution from the donor molecules is not significant. However, the former is much larger than that estimated from the two isolated spins of $S = 3/2$ ($Co^{2+}$), which is 3.75 emu K $mol^{-1}$, most plausibly due to the spin−orbital coupling of $Co^{2+}$.[20a] The magnetic properties of **5** were similar to those of (*N*-methylmorpholinium)$_2CoCl_4$, which shows significant discrepancy between the observed data and the behavior predicted by the spin 3/2 model.[20b,c] However, to date, no model is available to fit the experimental data of **5**.

**Comparison between the Head-to-Tail and Head-to-Head Stacks.** The asymmetric TTF derivatives acquire the freedom to form head-to-tail and/or head-to-head arrangements as mentioned in the introduction. For MeEDO-TTF salts, the stacking type has been limited to the latter arrangement as observed in (MeEDO-TTF)$_2$X (X = $BF_4^-$, $ClO_4^-$, $PF_6^-$), where the donors slip along the molecular short axis to show RoA type overlap (intermolecular interaction of $s$ in Figure 13a). The orientation of MeEDO-TTF molecules between the neighboring columns (interaction $p$ in Figure 13a) is reversed. Furthermore, the largest magnitude was observed along the side-by-side direction ($t$). As a result of the comparable overlap integrals ($t \approx 10 \times 10^{-3}$, $p \approx 9 \times 10^{-3}$, $s \approx 5 \times 10^{-3}$), the calculated Fermi surfaces showed 2D features. In other words, the suppression of face-to-face intermolecular interaction due to the geometrically poor overlap of the molecular orbitals in the head-to-head stacking provided 2D electronic structures.

Contrary to above, efficient face-to-face intermolecular interactions were observed in the head-to-tail stacks. The donor molecules showed almost no slip along the molecular short axis in the salts reported in this article (Figure 13b). The magnitudes of the intermolecular face-to-face overlap integrals were $23-46 \times 10^{-3}$. Especially, the RoR type overlap provided the largest magnitude of more than $30 \times 10^{-3}$. In these salts, the intermolecular overlap integrals along the molecular short axis were comparable to those in the head-to-head type stacking as mentioned above. The Q1D electronic structure of the columnar stack in **2** and localization of charge carriers in donor tetramers in **3** and **4** and most plausibly in dimers in **5** and **6** are not originated from the suppression of the intermolecular interactions along the molecular short axis but due to the much more efficient face-to-face interactions. It is worth noting that the RoR pairs are frequently formed in the salts reported here, while this type of donor packing is rarely found in the salts of TTF derivatives having substituents.[17b,c]

The donor layers purely consisting of head-to-head stacking of the asymmetric TTF analogues have only been reported for the salts of EDO-TTF and MeEDO-TTF. As a result of the small number of examples, it has been difficult

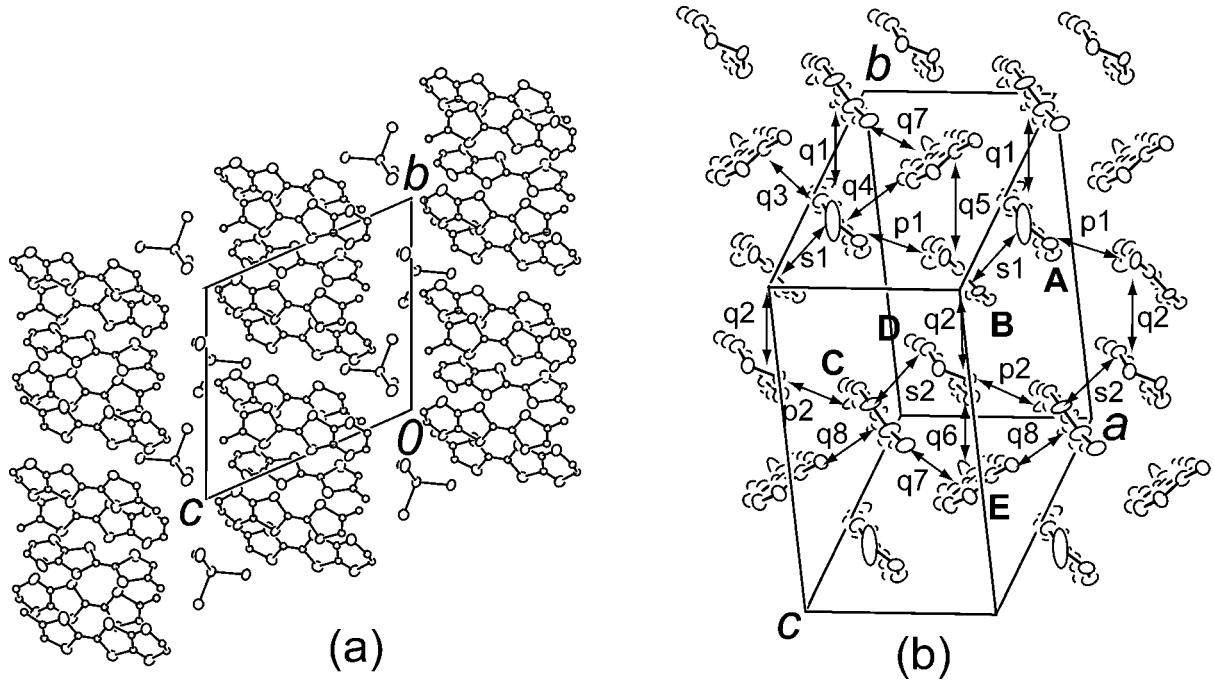


**Figure 10.** Crystal structure of **6**. The hydrogen atoms were omitted for clarity. (a) Projection along the *a*-axis (see Figure S20 in Supporting Information for the stereoview); (b) molecule arrangement of the conducting layer viewed along the molecular longitudinal axis. $s1 = 46.0$, $s2 = -45.0$, $p1 = 14.1$, $p2 = -14.0$, $q1 = -7.9$, $q2 = -10.3$, $q3 = -11.1$, $q4 = -2.4$, $q5 = -0.1$, $q6 = -2.8$, $q7 = -9.4$, $q8 = -3.8 \times 10^{-3}$.

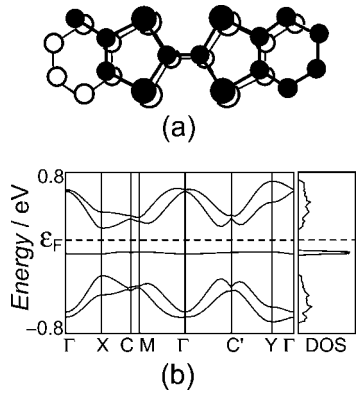


**Figure 11.** (a) Intradimer RoR type overlap in **6** between **A** and **B** (and **C** and **D**). The stereoview of the overlap modes was shown in Figure S21 in Supporting Information; (b) calculated band dispersion and DOS based on the crystal structure of **6** at room temperature.

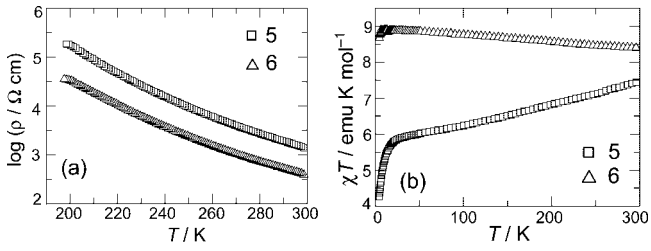


**Figure 12.** Temperature dependence of the resistivities (a) and magnetic susceptibilities (b) of **5** and **6**. The conductivities were measured on the single crystals by the conventional four-probe method.

to overview the effect of the molecular stacking on the electronic structure for the salts of asymmetric TTF derivatives. At the present stage, however, our results suggest that the head-to-head stacking of the asymmetric TTF analogues with small $\pi$-electron system more likely affords 2D electronic structures, while the head-to-tail stacking tends

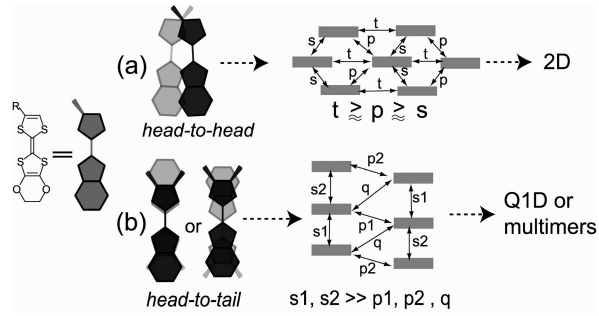


**Figure 13.** Schematic representation of the relationship between the intermolecular overlap mode, the donor packing arrangement viewed along the molecular longitudinal axis, and the dimensionality of the electronic structure (left to right). For the head-to-head overlap mode (a), the stacking column is defined as the one connected by the interaction *s*. In the indication of the molecular overlap modes for head-to-tail pairs (b), methyl groups were depicted in two positions per donor molecule to show the possible positional disorder in the salts.

to provide low dimensional electronic structures by forming tight 1D columns or localized charge carriers encapsulated in multimers. Further synthetic and analytical investigations of the radical cation salts with the head-to-head stacking, as well as the head-to-tail stacking, of other asymmetric TTF derivatives are needed to confirm this point.

## Conclusion

Six radical cation salts of MeEDO-TTF were prepared through electrocrystallization. Among these salts, $(MeEDO\text{-}TTF)_2ReO_4$ afforded three modifications to show different transport and magnetic properties. Except for the powder modification of $(MeEDO\text{-}TTF)_2ReO_4$ (**1**), the crystal structures of the salts were solved. Although the molecular arrangements showed a variety of patterns, including one-dimensional columns, $\kappa$-4 $\times$ 4 type tetramers, and the

coexistence of dimer and monomer, only the head-to-tail type arrangements were found for the face-to-face stacking pair of the donor molecules in these salts. The overlap modes in these donor pairs were classified into two kinds: "ring-over-bond" and "ring-over-ring" types, the latter of which has been found very seldom in the salts of TTF derivatives except for those of nonsubstituted TTF.

Compared with head-to-head type stacking observed in $(MeEDO\text{-}TTF)_2X$ ($X = BF_4^-$, $ClO_4^-$, $PF_6^-$), the intermolecular face-to-face overlap integrals in the head-to-tail type stacking were greatly enhanced and much larger than the interactions along the molecular lateral directions, especially when the overlap mode is "ring-over-ring" type. As a result, the head-to-tail stacking provided the columnar stack or multimers, in which the charge carriers are more or less isolated. These results suggest that the electronic structures of the radical cation salts of asymmetric donor molecule, MeEDO-TTF, can be estimated from their stacking patterns: head-to-tail type stacking more likely provides Q1D band structures or multimers with localized charge carriers, while the head-to-head one affords 2D electronic structures.

## Experimental Section

**General Details.** Electrolytes $(Bu_4N)ReO_4$, $(Bu_4N)_2(HCTMM)$, $(Et_4N)_2CoCl_4$, and $(Et_4N)_2MnCl_4$, were recrystallized from the appropriate solvents. EtOH was distilled from $Mg/I_2$ and stored under nitrogen atmosphere. In an H-shaped cell with a glass frit separating two chambers, MeEDO-TTF and electrolyte were placed in the anodic and both chambers, respectively. After dissolving the donor and supporting electrolyte under nitrogen, a constant current was applied between the platinum electrodes of the diameters of 2 and 1 mm for the anode and cathode, respectively. In a typical procedure, the donor (ca. 10 mg) and supporting electrolyte (ca. 100 mg) were dissolved in 18 mL of EtOH. The electro-oxidation applying 0.5 $\mu$A for 2 weeks afforded the radical cation salts as black powder or crystals. Although the conditions were varied to improve the crystal quality, relatively poor grade of products was obtained for **3** and **4**. For **3**, only the electrocrystallization at 5 °C afforded the needle crystals which could be used for the X-ray single crystal diffraction measurement, while the high current (10 $\mu$A) electrooxidation at room temperature afforded the long needle-like crystals with poorer quality. For **4**, only the very thin platelet crystals were obtained up to now, which were used for the X-ray diffraction measurement.

IR and UV−vis spectra measured on KBr pellets were recorded on Perkin-Elmer Paragon 1000 and Shimadzu UV-3100 spectrometers, respectively. The resistivities were measured through the conventional four- and two-probe methods for high and low temperature regions, respectively. For **1** and **4**, the resistivities were measured on the compressed pellets, which were prepared by applying the pressure around 18 kgf/cm$^2$, and cut to rectangular shape with the size of $1.4 \times 0.5 \times 0.2$ mm$^3$. The gold wires ($\phi = 25$ $\mu$m) were contacted with the surface of the sample by using carbon paste (DOTITE XC-12, JEOL; solvent: diethyl succinate, TCI). The resistivities of **2**, **3**, **5**, and **6** were measured on the single crystals. The gold wires ($\phi = 10$ $\mu$m) were contacted with the surface of the sample by using carbon paste. The cooling rate was 0.5 K min$^{-1}$. Liquid nitrogen was employed as the reference for the thermocouple of the temperature controller. The lowest temperature we measured was 10 K, which is the limitation of our apparatus. The temperature dependence of the magnetic susceptibility of **1**, **3**, **4**, **5**, and **6** was measured on the SQUID magnetometer of Quantum Design MPMSR2-XL applying the magnetic field of 10 kOe for **1**, **3**, and **4** and 1 kOe for **5** and **6**. The core diamagnetisms were estimated from the sum of Pascal constants amounting to $-3.27$ and $-3.01 \times 10^{-4}$ emu mol$^{-1}$ for **1** and **4**, respectively,[21] while that of **3** was estimated by the least-squares fitting applying a singlet−triplet model to be $-3.11 \times 10^{-4}$ emu mol$^{-1}$. The core diamagnetisms of **5** and **6** were neglected, since the core diamagnetisms for both salts were around 2% of their total susceptibilities. The magnetic property of **2** was measured on a single crystal ($1.4 \times 0.3 \times 0.05$ mm$^3$) through ESR (JEOL JES-TE200 X-band ESR spectrometer with $TE_{011}$ cavity) in the temperature range of 4−295 K. At room temperature, a Dysonian shaped resonance signal was observed when the static magnetic field was applied parallel to the *ac*-plane, for which the *g*-factor and line width were derived according to ref 22 (Figures S7 and S8 in Supporting Information). The ESR spectra showed a single Lorentzian signal in the entirety of the temperature region examined when the magnetic field was applied parallel to the donor molecular short and long axes, respectively. These orientations were employed to determine $\chi_{spin}$, which was derived by comparing the integral intensity of **2** with that of $CuSO_4 \cdot 5H_2O$. (Along with the *g*-factor and line width, temperature dependences of $\chi_{spin}$ determined by applying static magnetic field in different directions are shown in Figures S9–S11 in Supporting Information).

The intermolecular overlap integrals between the donor molecules were calculated by means of the extended Hückel method on the basis of the crystal structures. The tight binding approximation afforded the dispersion relation and the Fermi surface under the assumption of $t = Es$, where $t$ represents the transfer integrals, $s$ the overlap integrals, and $E = -10$ eV. The $\zeta$-parameters of atomic orbitals were taken from ref 3c for oxygen and from ref 23 for other atoms. The 3d orbitals of sulfur atoms were included in the calculation.

**X-ray Structure Determination.** The data were collected on an imaging plate type diffractometer (MacScience DIP-2020K) with graphite monochromated Mo K$\alpha$ radiation. The temperature for the X-ray data collection of **2** was controlled by a XR-CS10K cryostat (Japan Thermal Engineering) with the cooling/heating rate of 0.5 K min$^{-1}$. The structures were solved by a direct method of SIR2004[24a] and refined by a full matrix least-squares method on $F^2$ by means of Shelxl-97.[24b] As a result of the small size of the single crystals, we could not collect enough numbers of diffractions having satisfactory signal-to-noise ratios for **3**, and **4** provided only relatively weak diffractions. Although the detailed comparison of the bond lengths and so forth cannot be discussed for these salts, the orientation of the donor molecules was determined unambiguously: no disorder in the mixed sites of methyl and ethylenedioxy groups was observed. Even the positional disorder of the methyl group on an ethylene moiety was not detected. Although the crystals for **5** and **6** are very close to the centrosymmetric $P\bar{1}$ space group, the crystal structures of both salts are assigned to be noncentrosym-

(20) (a) Carlin, R. L. *Magnetochemistry*; Spinger: Berlin, 1986. (b) Parent, A. R.; Landee, C. P.; Turnbull, M. M. *Inorg. Chim. Acta* **2007**, *360*, 1943–1953. (c) Parent, A. R.; Turnbull, M. M., personal communication.
(21) Gupta, R. R. In *Landolt-Bornstein, New Series II*; Hellwege, K.-H., Hellwege, A. M., Eds.; Springer Verlag: Berlin, 1986; Vol. 16 (Diamagnetism Susceptibility).
(22) Chapman, A. C.; Rhodes, P.; Seymour, E. F. W. *Proc. Phys. Soc. B* **1957**, *70*, 345–360.
(23) Summerville, R. H.; Hoffmann, R. *J. Am. Chem. Soc.* **1976**, *98*, 7240–7254.
(24) (a) Burla, M. C.; Caliandro, R.; Camalli, M.; Carrozzini, B.; Cascarano, G. L.; de Caro, L.; Giacovazzo, C.; Polidori, G.; Spagna, R. *J. Appl. Crystallogr.* **2005**, *38*, 381–388. (b) Sheldrick, G. M. *SHELXS-97-A Program for Crystal Structure Refinement*; University of Göttingen: Göttingen, Germany, 1997; Release 97-2.

**Table 3. Crystallographic Data, Data Collection, and Reduction Parameters of the Needle Modification of (MeEDO-TTF)$_2$ReO$_4$ (3) along with Those of 4, 5, and 6 for Room Temperature Measurements**

| | 3 | 4 | 5 | 6 |
|---|---|---|---|---|
| chemical formula | $C_{36}H_{32}O_{16}Re_2S_{16}$ | $C_{46}H_{32}N_6O_8S_{16}$ | $C_{45}H_{40}Cl_8Co_2O_{10}S_{20}$ | $C_{45}H_{40}Cl_8Mn_2O_{10}S_{20}$ |
| formula weight | 1605.98 | 1309.85 | 1783.62 | 1775.45 |
| crystal system | monoclinic | monoclinic | triclinic | triclinic |
| space group | $P2_1/n$ (No. 14) | $P2_1/a$ (No. 14) | $P1$ (No. 1) | $P1$ (No. 1) |
| crystal size, mm$^3$ | 0.5 × 0.05 × 0.03 | 0.5 × 0.1 × 0.03 | 0.5 × 0.2 × 0.05 | 0.5 × 0.2 × 0.03 |
| $a$, Å | 8.415 (2) | 8.382 (1) | 8.351 (1) | 8.383 (1) |
| $b$, Å | 21.170 (4) | 21.511 (2) | 14.372 (1) | 14.457 (1) |
| $c$, Å | 29.326 (6) | 16.292 (2) | 15.421 (2) | 15.359 (2) |
| α, deg | | | 112.353 (6) | 111.965 (6) |
| $\beta$, deg | 90.60 (3) | 97.587 (6) | 100.095 (7) | 99.799 (7) |
| $\gamma$, deg | | | 96.184 (6) | 96.161 (6) |
| $V$, Å$^3$ | 5224 (2) | 2911.8 (4) | 1654.1 (3) | 1671.1 (3) |
| $Z$ | 4 | 2 | 1 | 1 |
| $\mu$, mm$^{-1}$ | 5.334 | 0.648 | 1.508 | 1.375 |
| $d_{calcd}$, g cm$^{-3}$ | 2.042 | 1.494 | 1.790 | 1.764 |
| radiation | Mo Kα | Mo Kα | Mo Kα | Mo Kα |
| $2\theta_{max}$, deg | 52.0 | 52.1 | 52.0 | 52.0 |
| no. of independent obsd reflections | 8227 | 4989 | 9738 | 10264 |
| no. of reflections with $I > 2\sigma(I)$ | 4940 | 3622 | 6499 | 8031 |
| no. of refined parameters | 683 | 358 | 767 | 768 |
| $wR2$[a] (for all data) | 0.257 | 0.345 | 0.160 | 0.145 |
| $R_{gt}$ (%) (for $I > 2\sigma(I)$) | 0.088 | 0.114 | 0.060 | 0.056 |
| GOF[b] | 1.019 | 1.374 | 1.043 | 1.045 |

[a] $W = 1/[\sigma^2F_o^2 + (\alpha P)^2 + \beta P]$, where $P = (F_o^2 + 2F_c^2)/3$; for **3**, α = 0.1234, $\beta$ = 51.8186; for **4**, α = 0.2000, $\beta$ = 0.0000; for **5**, α = 0.0615, $\beta$ = 3.2908; for **6**, α = 0.0424, $\beta$ = 2.7045. [b] Calculated for all of the independent reflections.

metric $P1$ space group since an asymmetric unit contains five MeEDO-TTF molecules and MeEDO-TTF is an acentric molecule. However, because of the limitation of our X-ray diffractometer, the obtained reflection data are highly correlated to each other. Therefore, in the structure refinement of **5** and **6**, the restraints of DFIX (1.35 0.02) were applied for the C═C bond lengths of all of the crystallographically unique MeEDO-TTF molecules to make the corresponding bond lengths in the reasonable range. Accordingly, the resulting C═C bond lengths could not be applied for the estimation of the charge on each molecular site. The positional parameters of the hydrogen atoms for **3**, **4**, **5**, and **6** were calculated under a fixed C−H bond length of 1.00 Å with sp$^2$ or sp$^3$ configuration of the bonding carbon atoms. In the refinement procedures, isotropic temperature factors with the magnitudes of 1.2 times to those of the equivalent temperature factors of the bonding carbon atoms were applied. The parameters for crystals, data collections, and refinements of **2** are summarized in Table 2, and those of **3**, **4**, **5**, and **6** are listed in Table 3.

**Acknowledgment.** The authors are grateful to Dr. A. R. Parent and Prof. M. M. Turnbull (Clark University, U.S.A.) for their kindness to offer the magnetism data of (*N*-methylmorpholinium)$_2$CoCl$_4$ salt and helpful comments on the magnetism of (MeEDO-TTF)$_5$(CoCl$_4$)$_2$. The authors thank Dr. Salvat Khasanov (Kyoto University, Japan) for his helpful comments about the crystal structures of the plate modification of (MeEDO-TTF)$_2$ReO$_4$. The authors also would express their thanks for Professor T. Mori (Tokyo Institute of Technology, Japan) for his kind information about the radical cation salts containing RoR type stack of the donor molecules. This work was partly supported by Grants-in-Aid for Scientific Research on Priority Areas of Molecular Conductors (No. 15073215), 21st Century COE on Kyoto University Alliance for Chemistry (No. 15205019), from the Ministry of Education, Culture, Sports, Science and Technology, Japan, and for Creative Scientific Research (18GS0208) from JSPS.

**Supporting Information Available:** Figures S1−S26: Stereoview of the intermolecular overlap mode in (MeEDO-TTF)$_2$X (X = $BF_4^-$, $ClO_4^-$, and $PF_6^-$); typical photos of the three modifications of the (MeEDO-TTF)$_2$ReO$_4$ salts; temperature dependences of the resistivity and magnetic susceptibility of **1**; stereoview of the intermolecular overlap modes in **2** at 300 K; stereoview of the intermolecular overlap modes of **2** at 150 K; calculated band structure of **2** based on the crystal structure at 150 K; detailed information of the ESR measurement of **2**; stereoview of a unit cell of **3** projected along the *a*-axis; stereoscopic view of the intratetramer intermolecular overlap modes in **3**; crystal structure and the scheme of the overlap integrals of **4**; anion arrangement in **4**; stereoview of the intermolecular overlap modes of **4**; calculated band structure of **4**; temperature dependences of the resistivity and magnetic susceptibility of **4**; stereoview of the crystal structure of **6** projected along the *a*-axis; stereoview of the intradimer RoR type overlap in **6**;crystal structure and the scheme of the overlap integrals of **5**; stereoview of the intermolecular overlap modes of **5**; and calculated band structure of **5** (PDF). Crystallographic data in CIF format. This material is available free of charge via the Internet at http://pubs.acs.org.

CM803180X